New Journal of Physics
The open-access journal for physics

Time-resolved mapping of correlated electron emission from helium atom in an intense laser pulse

C Ruiz and A Becker[1]
Max-Planck-Institut für Physik of Komplexer Systeme, Nöthnitzer Str. 38, D-01187 Dresden, Germany
E-mail: abecker@pks.mpg.de

New Journal of Physics **10** (2008) 025020 (12pp)
Received 10 September 2007
Published 29 February 2008
Online at http://www.njp.org/
doi:10.1088/1367-2630/10/2/025020

Abstract. We apply and analyze the concept of mapping ionization time on to the final momentum distribution to the correlated electron dynamics in the nonsequential double ionization of helium in a strong laser pulse ($\lambda = 800$ nm) and show how the mapping provides insight into the double ionization dynamics. To this end, we study, by means of numerical integration of the time-dependent Schrödinger equation of a fully correlated model atom, the temporal evolution of the center-of-mass momentum in a short laser pulse. Our results show that in the high intensity regime ($I_0 = 1.15 \times 10^{15}\,\mathrm{W\,cm^{-2}}$), the mapping is in good agreement with a classical model including binary and recoil rescattering mechanisms. In the medium intensity regime ($I_0 = 5 \times 10^{14}\,\mathrm{W\,cm^{-2}}$), we identify additional contributions from the recollision-induced excitation of the ion followed by subsequent field ionization (RESI).

Contents

[1] Author to whom any correspondence should be addressed.

1. Introduction

The typical timescale of electron motion in an atom is a few tens of attoseconds, which is shorter than a single period of the electric field at optical and near-infrared (IR) wavelengths. Nevertheless, several recent experiments have demonstrated that such fields can be used, sometimes in combination with attosecond pulses at XUV wavelengths, to detect and control electron motion on the attosecond timescale (for a review, see [1]). For example, it has been shown that it is possible to measure directly the electric field of a light pulse using the subcycle dynamics of the electron [2]. Furthermore, a method named orbital tomography has been introduced, in which an image of an electronic orbital in a molecule has been measured using attosecond bursts of light [3]. These measurements are closely related to the experimental progress in the generation of attosecond pulses of coherent XUV radiation (for reviews, see [1, 4]), which promise to open the route to time-resolved atomic physics, as the temporal width of the pulses is comparable with the electron motion on the atomic scale.

Parallel to this progress, another hot topic in strong field physics is the analysis of correlated electron dynamics driven by an intense laser field. An important example is the correlated electron emission from an atom or molecule in the field, also called non-sequential double ionization (NSDI) (for a review, see [5]). It is nowadays widely accepted that the mechanism for this process at optical and near-IR wavelengths is based on the so-called rescattering scenario [6]. According to this picture, one electron tunnels through the combined barrier of the field and the Coulomb potential of the atom or molecule. It is then driven by the oscillating electric field of the laser and can rescatter with the parent ion to liberate a second electron in an inelastic collision. The electric field acts in this process as a clock starting with the excitation of the first electron to the continuum near the maximum of the field and stopping with the recollision about $3/4$ of a cycle later near a zero of the field. It is well known that the recollision event extends over a few hundred attoseconds in time and is hence well confined in time. A second related pathway to NSDI is the excitation of the parent ion induced by the recollision of the first electron and the subsequent ionization of the second electron from the excited ion, also called RESI [7]. Again, the secondary electron emission process is confined to a period in time much shorter than a field cycle, here around a maximum of the field. We may note that both pathways have also been identified in elaborate calculations using S-matrix theories (for a review, see [8]) and numerical model calculations (e.g. [9, 10]).

The goal of this paper is to analyze, using the results of numerical simulations, how these subfemtosecond events are mapped on to the final momentum distribution of the two electrons. Due to the temporal confinement of the correlated electron emission via different pathways to discrete times in a field cycle, it is expected (e.g. [7, 11, 12]) that information about the mechanisms can be inferred from the experimental observations at the end of an ultrashort few-cycle pulse. In the numerical simulations the mapping principle can be tested by inspecting the temporal evolution of the correlated electron emission. To this end, we explore double ionization by a strong laser pulse of a few cycles at the Ti:sapphire wavelength and two peak intensities ($I_0 = 5 \times 10^{14}$ and $1.15 \times 10^{15}\,\mathrm{W\,cm^{-2}}$). Our analysis is based on the numerical integration of the time-dependent Schrödinger equation (TDSE) for the correlated wavefunction in a two-electron model atom. In the model [9, 10], the center-of-mass motion of the two electrons is restricted to the polarization direction, while the relative motion of the electron remains unrestricted. Therefore the electron–electron interaction term is fully taken into account, which puts the model beyond the often used one-dimensional (1D) model [13], in which the motion

of each electron and, hence, the electron–electron interaction is restricted to the polarization direction.

The paper is organized as follows: first, we sketch the concept of mapping of attosecond single electron dynamics on to the final momentum distribution and discuss its extension to the correlated electron emission via the center-of-mass momentum of the two electrons. Next, we use it to get insights into the temporal evolution of the correlated electron dynamics by analyzing numerical results for the NSDI process in two different intensity regimes. For the interpretation of the quantum calculations, we further use a simple classical model. We end by summarizing the results concerning the subfemtosecond nature of the double ionization events.

2. Mapping of subfemtosecond ionization dynamics on to momentum distributions

The main characteristics of the photoelectron momentum spectra in a strong laser field can be roughly understood by means of simple classical considerations. Assuming that the electron is excited to the continuum at time t_i with zero velocity and neglecting the atomic potential, the electron will move as a free particle under the influence of the laser field only. For a pulse which is switched off adiabatically, the classical equations for the momentum of the electron along the polarization direction, $p_{1,z}$, can be easily integrated, leading to (we use Hartree atomic units, $e = m = h = 1$)

$$p_{1,z}(t \to \infty) = -\int_{t_i}^{\infty} E(t)\mathrm{d}t = -\frac{A(t_i)}{c}, \tag{1}$$

where $A(t) = -c\int^t E(t')\,\mathrm{d}t'$ is the vector potential and $E(t)$ the electric field. The expression shows that the final momentum of the electron under the above assumptions depends on the ionization time t_i only. Here, ionization time refers to the real time of removal of the electron from the core. This time is also used for the integration of the classical equations of motion presented below.

The general principle underlying this interpretation, namely the mapping of time to momentum or energy by means of a fast ionization event and a streaking via an oscillating electric field of a laser pulse, is exemplified in figure 1. An important application is the attosecond streak camera [14]. In this technique, an attosecond XUV pulse ionizes an atom by a one-photon absorption and a second low intensity IR laser pulse is used to change the final momentum of the emitted electron. The basic principle has also been used to measure the electric field of a near-IR ultrafast laser pulse [2] and the duration of attosecond pulses with the FROGCRAB technique [15]. In the ideal case, the mapping can be reversed to infer from the final momentum of the electron its release time. For long pulses, in which the envelope of the pulse has almost the same amplitude over several cycles, ionization events separated by one cycle are mapped to the same final momentum and the release phase inferred is relative to the laser cycle only (cf figure 1, left-hand panel). In contrast, when a short pulse is used, individual ionization events arising from different cycles might become distinguishable (figure 1, right-hand panel).

The principle can be extended to the case of (correlated) emission of two (or more) electrons using the streaking of the center-of-mass of an electron pair. Assuming that single ionization occurs at time t_0, while at some later time t_1 in the pulse the second electron is set free, the center-of-mass momentum of the two electrons in the direction of the polarization

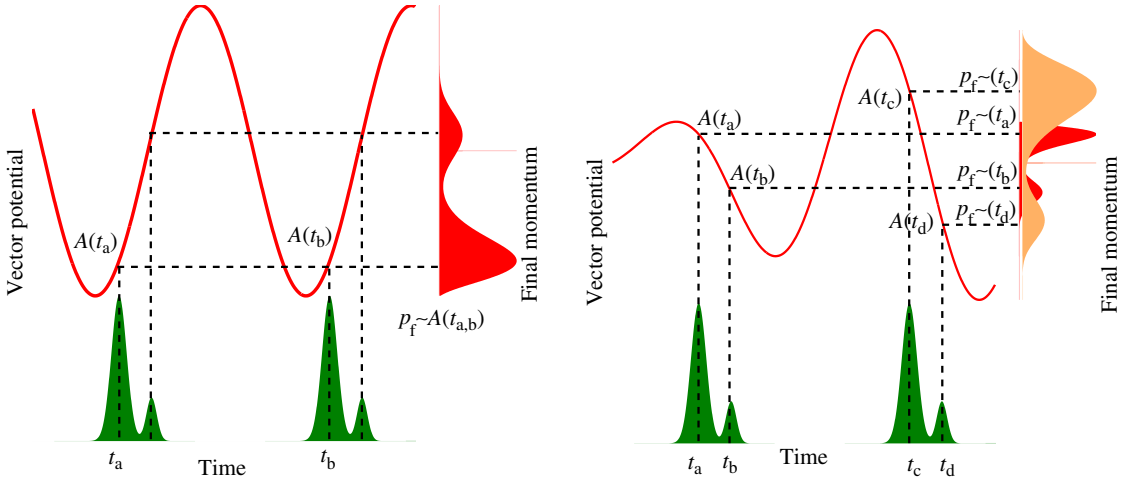

Figure 1. Mapping of the ionization time to the final momentum of the electron. If an ionization event is short compared to the period of the laser field, the value of the final momentum of the electron is expected to be well approximated by the value of $A(t_i)$ where t_i is the time of electron emission. Left-hand panel: in the case of a long pulse, two ionization events separated by one laser cycle will be mapped on to the same final momentum. Right-hand panel: for a short laser pulse, each ionization event is mapped on to a different final momentum and the events can be distinguished in the momentum distribution.

direction of the field is given by:

$$P_z(t \to \infty) = -\int_{t_0}^{t_1} E(t)\mathrm{d}t - 2\int_{t_1}^{\infty} E(t)\mathrm{d}t - \Delta p_z = -\frac{A(t_0) + A(t_1)}{c} - \Delta p_z. \tag{2}$$

Δp_z accounts for the possibility of a momentum transfer of the first electron to the ion. For sequential double ionization or a shake-off process, the momentum transfer is negligible ($\Delta p_z = 0$). On the other hand, in the rescattering scenario, the first electron will, most likely, transfer energy and momentum to the ion at the instant of its return. One may estimate the energy transfer either by the excitation energy of the second electron (e.g. to the first excited state of the ion) in the case of the RESI process or by the ionization energy of the second electron in the case of a direct ionization upon rescattering of the first electron with the ion. We will use the latter estimation in the classical model calculations below. It is seen from equation (2) that the final center-of-mass momentum depends on both time instants t_0 and t_1. As discussed at the outset, in the recollision scenario the first step is the emission of one electron near the maximum of the field, i.e. $A(t_0) \simeq 0$. Thus, the center-of-mass momentum is determined in this approximation by the vector potential at time t_1, at which the second electron is excited to the continuum, and the momentum transfer Δp_z.

In numerical simulations, the mapping principle can be explicitly tested by obtaining the canonical center-of-mass momentum as a function of time. For calculations in velocity gauge the canonical momentum corresponds at each time to the final momentum outside the field. An analysis of the temporal evolution of the center-of-mass momentum will therefore provide (i) a test of the mapping principle in equation (2) and (ii) insights into the double ionization dynamics. To this end, we have integrated numerically the TDSE for the case of the helium atom

interacting with a few-cycle intense laser pulse and analyze the numerical results for the center-of-mass momentum as a function of time.

3. Numerical model

For our numerical analysis, we have used a recently introduced two-electron model [9, 10] and applied it to the case of the helium atom interacting with a few-cycle laser pulse. We consider the TDSE in the reference frame of the center-of-mass and the relative coordinates of the two electrons. The two-electron Hamiltonian of the system can then be written in the dipole approximation as:

$$H(\mathbf{R}, \mathbf{r}, t) = \frac{\mathbf{P}^2}{4} + \mathbf{p}^2 - \frac{\mathbf{P}\cdot\mathbf{A}(t)}{c} + \frac{1}{r} - \frac{2}{|\mathbf{R} + (\mathbf{r}/2)|} - \frac{2}{|\mathbf{R} - (\mathbf{r}/2)|}, \tag{3}$$

where $\mathbf{R} = (\mathbf{r}_1 + \mathbf{r}_2)/2$, $\mathbf{P} = \mathbf{p}_1 + \mathbf{p}_2$, $\mathbf{r} = \mathbf{r}_1 - \mathbf{r}_2$ and $\mathbf{p} = (\mathbf{p}_1 - \mathbf{p}_2)/2$ are the center-of-mass and relative coordinates and associated momenta, respectively. In this reference frame, the two main interactions for NSDI, namely the electron–field interaction and the electron correlation, are decoupled in the two coordinates. We now take advantage of the fact that in an intense linearly polarized laser field the electron–field coupling is strongly directed along the polarization axis and therefore restrict the center-of-mass motion along this direction ($\mathbf{P} \to P_Z$, $\mathbf{R} \to Z$). The final model Hamiltonian for the helium atom therefore depends on three degrees of freedom as follows:

$$H = \frac{P_Z^2}{4} + p_z^2 + p_\rho^2 - \frac{P_Z A(t)}{c} + \frac{1}{\sqrt{z^2+\rho^2}} - \frac{2}{\sqrt{(Z - z/2)^2 + \rho^2/4 + a^2}} - \frac{2}{\sqrt{(Z + z/2)^2 + \rho^2/4 + a^2}}, \tag{4}$$

where z and ρ represent the relative coordinates of the two electrons parallel and perpendicular to the polarization axis. The parameter a^2 is introduced to soften the attractive Coulomb potentials in the numerical calculations. With $a^2 = 0.135$, the ground-state energies of neutral helium and the helium ion are -2.936 and -1.985 au, respectively.

The numerical propagation of the wavefunction is done using the Cranck–Nicholson scheme on a grid. For the computations, we have chosen a N-cycle laser pulse with $E(t) = E_0 \sin^2(\omega t/2N)\sin(\omega t)$, and a carrier frequency of $\omega = 0.057$ au, which corresponds to the Ti:sapphire laser wavelength of 800 nm. Two peak intensities have been considered, namely $I_0 = 5 \times 10^{14}$ and $1.15 \times 10^{15}\,\mathrm{W\,cm^{-2}}$ with $N = 4$ in each pulse. We have used a numerical grid with $N_Z = 2000$ (3000), $N_z = 1000$ (1500) and $N_\rho = 200$ (300) points for the low (high) intensity case. In all simulations, the grid spacing was $\Delta Z = \Delta z = \Delta\rho = 0.3$ au and the time step was $\Delta t = 0.05$ au.

For the momentum analysis of the two correlated electrons in the continuum, we have partitioned the coordinate space as [9]

$$r_1 < 12\,\text{au} \quad \text{and} \quad r_2 < 12\,\text{au} \quad : \quad \text{He atom}, \tag{5}$$

$$r_1 < 6\,\text{au} \quad \text{and} \quad r_2 \geqslant 12\,\text{au} \quad \text{or} \quad r_1 \geqslant 12\,\text{au} \quad \text{and} \quad r_2 < 6\,\text{au} \quad : \quad \text{He}^+ \text{ ion}, \tag{6}$$

$$\text{complementary space} \quad : \quad \text{He}^{2+} \text{ ion}, \tag{7}$$

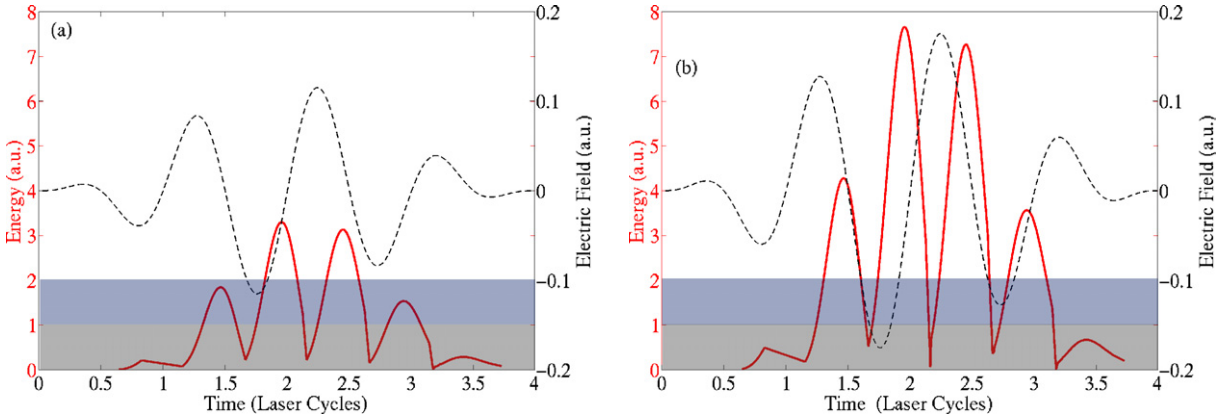

Figure 2. Energy E of the first electron at the instant of rescattering according to the semiclassical three-step model (solid line; [6]) at peak intensities of (a) $I_0 = 5 \times 10^{14}\,\mathrm{W\,cm^{-2}}$ and (b) $I_0 = 1.15 \times 10^{15}\,\mathrm{W\,cm^{-2}}$; also shown is the electric field (dashed line). The zones of different colors separate the energy regimes for excitation and ionization of the ion.

with $r_1 = \sqrt{(Z + (z/2))^2 + (\rho^2/4)}$ and $r_2 = \sqrt{(Z - (z/2))^2 + (\rho^2/4)}$. The distribution of the center-of-mass momentum along the polarization direction has been obtained by taking the Fourier transform of the double ionization part and integrating over the components of the relative coordinate. Please note that these distributions correspond to the canonical center-of-mass momentum, which corresponds at each time to the momentum observed outside the field at the end of the pulse.

4. Double ionization dynamics at different intensities

As outlined above, in this section we will analyze the center-of-mass momentum distribution of the two electrons as a function of time, obtained from the double ionization part of the wavefunction. We have considered peak intensities in the medium and high intensity regimes. According to the semiclassical rescattering scenario [6], the return energies of the first singly ionized electron differ considerably, as can be seen from figure 2. The energies are obtained simply by integrating the classical equations of the 1D motion with the electric field only. We have considered the release of an electron with zero velocity at the origin at different time instants in the laser cycle. In the case that the classical motion leads to a return of the electron to the origin, the return energy has been obtained and is plotted as a function of the return (recollision) time in figure 2. The zones of different colors separate the energy regimes, in which the energy of the returning electron exceeds the limits for excitation (gray zone) and ionization (white zone) of the residual ion. Taking into account that the ionization probability is largest at the two maxima of the pulse, we may expect that the last two rescattering events around $t = 2.5T$ ($t = 275\,\mathrm{au}$) and $t = 3T$ ($t = 325\,\mathrm{au}$) will generate the largest contributions to the double ionization signal. According to the classical analysis, at the higher intensity in both events the electron energy should be sufficient to lead to direct ejection of the second electron upon rescattering, while at the medium intensity in the last rescattering event, only excitation of the ion should be possible.

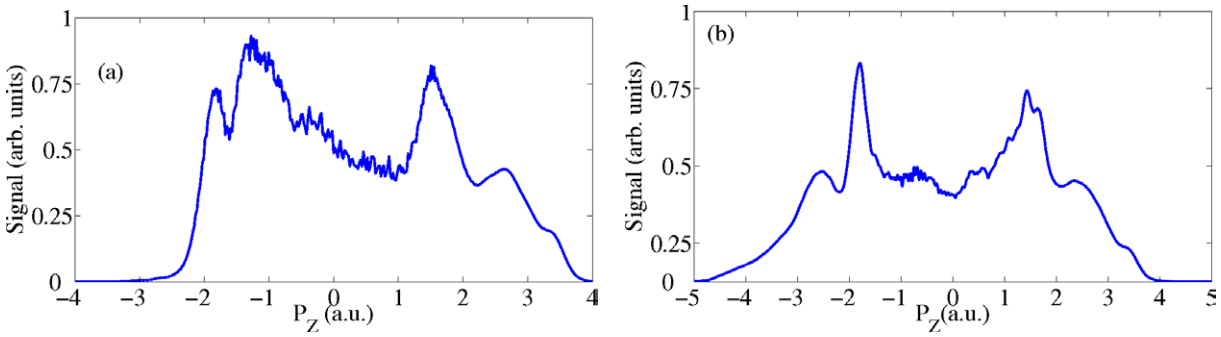

Figure 3. Final distributions of the center-of-mass momentum at (a) $I_0 = 5 \times 10^{14}\,\mathrm{W\,cm^{-2}}$ and (b) $I_0 = 1.15 \times 10^{15}\,\mathrm{W\,cm^{-2}}$.

Before turning to the aspect of mapping of ionization time into the center-of-mass momentum, we first present the final distributions of the center-of-mass momentum at the end of the pulse for the two intensities in figure 3. In both cases we observe a double hump structure with two major peaks at about $P_Z = \pm 1.4$ au for $I_0 = 5 \times 10^{14}\,\mathrm{W\,cm^{-2}}$ (panel a) and $P_Z = \pm 1.8$ au for $I_0 = 1.15 \times 10^{15}\,\mathrm{W\,cm^{-2}}$ (panel b) with a central minimum in between. The distributions are asymmetric over $P_Z = 0$ au due to the ultrashort pulse used in the simulations. According to the common interpretation, as has been proposed in previous classical analysis of experimental data [7, 11, 12], the two peaks are related to emission of the second electron upon rescattering at a zero of the field (maximum of the vector potential), while the center of the distribution results from the so-called RESI process, in which the second electron is released at the maxima of the field from an excited state of the ion. Please note that, in general, the RESI process can also contribute to the two humps [7], which are however usually neglected in the interpretation. It is the aim of the present paper to confront this interpretation with results of numerical simulations on the temporal evolution of the center-of-mass momentum distribution during the pulse.

Before we proceed, we may note that in figure 3 the central minimum in the distribution is slightly deeper in the high intensity case as compared to medium peak intensity. This result is in agreement with the general expectation and experimental observation that the relative strength from the RESI process to that of the direct emission process decreases as the laser intensity increases. We may, however, stress that in the present numerical simulations some contributions to double ionization, created early in the pulse, are being absorbed at the boundaries of the grid before the end of the calculation. This does influence the asymmetry in the relative heights of the two humps as well as the ratio of the heights of the humps to the central minimum. Therefore, the present results cannot be used as a quantitative prediction for future experiments, but just for a qualitative analysis of the double ionization dynamics. Finally, please note the occurrence of two small side peaks at larger momenta in both distributions. As we will show below, they do not follow the simple mapping principle, equation (2), and may result from an additional interaction of one of the electrons with the core [16].

4.1. Mapping at high intensity

We will now test the general expectations and common interpretation about the ionization times, as they have been inferred in previous works from the final distribution, by analyzing

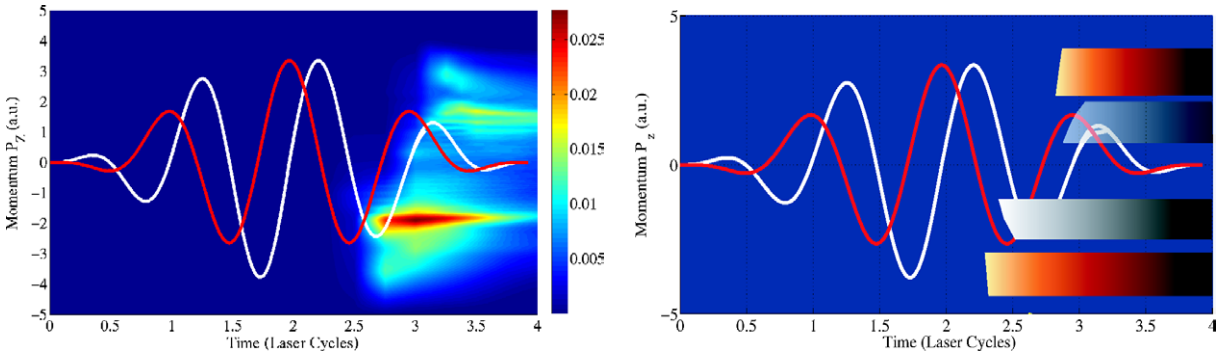

Figure 4. Left-hand panel: evolution of the center-of-mass momentum as a function of time for a peak intensity of $I_0 = 1.15 \times 10^{15}\,\mathrm{W\,cm^{-2}}$. Two main recollision events account for the final momentum distribution. Right-hand panel: momentum regimes for binary (gray zones) and recoil collisions (red zones) as obtained from classical calculations. Also shown are the (scaled) electric field (white line) and the vector potential (red line).

the temporal evolution of the center-of-mass momentum distribution during the pulse from the numerical results. We first consider the case of high intensity at $I_0 = 1.15 \times 10^{15}\,\mathrm{W\,cm^{-2}}$. The corresponding temporal evolution of the canonical center-of-mass momentum distribution, as it is obtained from the doubly ionized part of the full wavefunction, is shown in figure 4 in the left-hand panel. The horizontal and vertical axes correspond to the time (scaled in units of the laser cycle) and the center-of-mass momentum of the two electrons, respectively. The color coding represents the population of the doubly ionized part of the wavefunction at a given momentum and instant of time. To guide further interpretation, also shown are the scaled electric field (white line) and the vector potential (red line) as a function of time.

While in the experiment the final momentum distribution is accessible after the pulse only, the numerical results in figure 4 provide further insights into how the final momentum distribution builds up during the pulse. It is clearly seen from figure 4 that the two humps in the final momentum distribution correspond to the two main rescattering events at about $t = 2.5T$ and $t = 3T$ near the end of the pulse. In the figure, the contributions appear with a short delay from their instant of generation. This is due to the partition of the coordinate space into different regions in the numerical simulations (cf equations (5)–(7)). In the case of direct emission of the second electron upon rescattering, both electrons are close to the nucleus when the doubly ionized wavepacket is created. According to our partition of the grid, the correlated wavepacket is accounted as a bound contribution until it has propagated some distance away from the nucleus and enters the doubly ionized region in the numerical simulations. We may infer the actual time of birth with a good approximation by extrapolating up to the line of the vector potential. We identify a major contribution at each of the two events, but there appears also a minor peak at slightly larger momenta. We may note that despite the fact that we have chosen a relatively large grid to keep most of the wavefunction on the grid up to the end of the pulse, parts of the double ionized wavepackets with high center-of-mass momenta got absorbed at the boundaries. This explains the partial decay of the contributions towards the end of the pulse.

The major contributions are seen to appear at momenta which are almost equal to the maxima of the vector potential at $t = 2.5T$ ($t = 275$ au) and $t = 3T$ ($t = 325$ au). This indicates that both contributions to double ionization are generated close to the zeros of the field, in agreement with the interpretation of a direct emission of the second electron upon rescattering of the first electron. This is in agreement with the common interpretation of the two-hump structure of the final center-of-mass momentum distribution (cf discussion of the results in figure 3). The interaction of the two electrons can be simply considered as a binary collision, well known from field-free electron impact ionization. As can be seen from figure 4 the contributions remain at almost constant momenta throughout the rest of the pulse. This is in agreement with the mapping principle that the final center-of-mass momentum is determined by the vector potential at the time of creation of the doubly ionized wavepacket. The evolution at constant momenta further shows that these contributions are dominantly driven by the interaction with the field, while the interaction with the Coulomb potential of the residual core seems to be negligible.

The relative strength of the two main contributions is also in agreement with the expectations of the semiclassical recollison scenario, since the probability of electron impact ionization near threshold rises with an increase of the impact energy (cf figure 2(b)). Note that the probability of single ionization should be almost the same in both events, as the first electron is born near either one of the two main maxima of the pulse.

We now turn to the contributions that appear at momenta larger than the maximum value of the vector potential. The occurrence of such large momenta indicates an additional interaction of at least one electron with the nucleus during the double ionization process. We interpret it as a signature of a recoil collision, in which, after the binary encounter between the two electrons the impacting electron is backscattered at the nucleus. This interpretation is also in agreement with recent experimental observations and numerical results of a finger-like structure in the correlated electron momenta distributions [16]. We may further note that the results seem to indicate that these minor contributions in the center-of-mass momentum distributions do not evolve at constant momentum, as is assumed in the mapping principle. The effect could, however, partially occur due to a quick absorption of these contributions with high momenta at the boundaries too. A decrease of the center-of-mass momentum with time would be another indicator of a strong electron–nucleus interaction.

In general, this high intensity case appears to be rather well understood in terms of the semiclassical analysis, taking into account the separation into binary and recoil collisions. The latter leads to previously unexpected large center-of-mass momenta beyond the classical expectations for a correlated electron pair born at the zero of the field (cf [16]). It is, however, straightforward to take the recoil collision into account in the classical considerations [16, 17]. One simply has to assume that the first electron delivers enough energy to liberate the second electron, which corresponds to $|\Delta p_z| = \sqrt{2I_\mathrm{p}}$ in equation (2) where I_p is the ionization potential of the He^+ ion. The electron then either continues to propagate with reduced momentum in the same direction as before (binary collision) or is reflected in the opposite direction (recoil collision). The kinematical constraints on the center-of-mass momentum for the two main rescattering events, shown in the right-hand panel of figure 4, are found to be in good agreement with the numerical results.

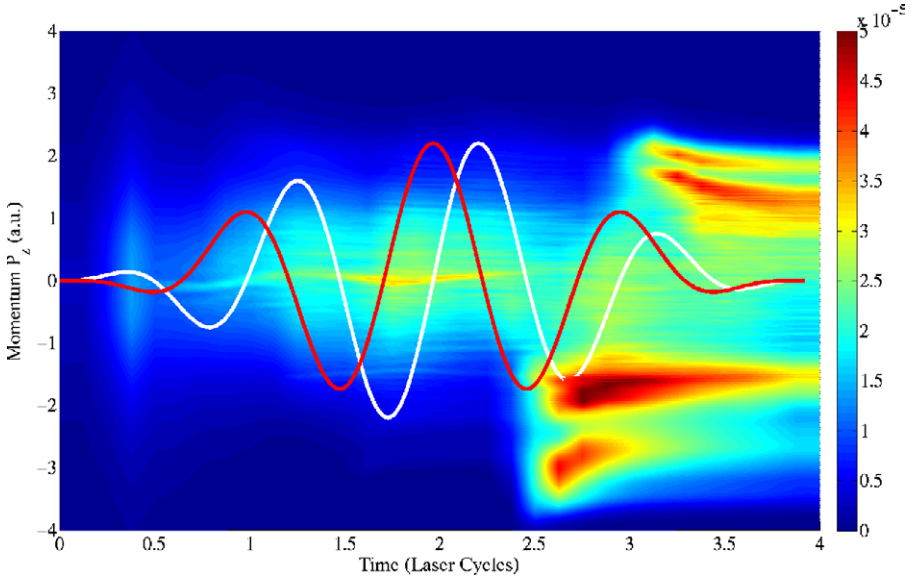

Figure 5. Evolution of the center-of-mass momentum as a function of time for a peak intensity of $I_0 = 5 \times 10^{14}\,\mathrm{W\,cm^{-2}}$. Two main recollison events account for the final momentum distribution. Also shown are the electric field (white line) and the vector potential (red line).

4.2. Mapping at medium intensity

We now turn to the double ionization dynamics at a lower intensity of $I_0 = 5 \times 10^{14}\,\mathrm{W\,cm^{-2}}$. The corresponding evolution of the center-of-mass momentum of the doubly ionized wavepackets is shown in figure 5. At first glance the evolution is more complex, but shows some similarities to the high intensity case discussed above.

We clearly see the occurrence and evolution of the two major contributions at $t = 2.5T$ ($t = 275\,\mathrm{au}$) and $t = 3T$ ($t = 325\,\mathrm{au}$) corresponding to the two humps and the side peaks in the final momentum distribution, which come from the last two rescattering events during the pulse. The signatures of these contributions are similar to those identified and discussed in the high intensity case. As before, a part of the contributions appears at momenta which correspond to the maxima of the vector potential at the time instants of recollision, while a second part occurs at larger momenta. The center-of-mass momentum of the former contributions does not change during the rest of the pulse (in accordance with the mapping principle), while the latter gets, here, clearly decelerated and ends at a lower momentum as it is created. Since we have performed the calculations with almost the same grid parameters as the high intensity calculations, absorption at the boundaries is, here, less important as the highest center-of-mass momenta are, here, considerably smaller than in the high intensity case. Thus, in this case, an interpretation of the decrease of the momenta as due to an electron–nucleus interaction appears to be even more obvious. We interpret the two contributions, as in the high intensity case, as due to binary and recoil collisions upon rescattering of the first electron. Please note that in the first of the two major rescattering events, the contributions of both the binary and the recoil collisions appear at almost the same time instant. In contrast, in the last rescattering event, the contribution from the binary collision appears with some time delay as compared to that of

the recoil collision. This might be connected to the fact that according to the simple classical estimation (cf figure 2(a)) the energy of the returning electron in the last rescattering event is not large enough to ionize the second electron and the double ionization has to be thought of as being assisted by the laser field.

In contrast to the high intensity case, we observe in figure 5 the occurrence and evolution of significant contributions at zero center-of-mass momentum throughout the pulse. These contributions are created near the maxima of the field, as is most clearly seen at $t = 1.25T$ ($t = 137$ au) and $t = 1.75T$ ($t = 192$ au), and evolve at constant center-of-mass momenta. They are in agreement with the predictions of the so-called RESI process [7], in which the first electron excites the ion upon rescattering and the second electron gets ionized from the excited state at the field maximum. Please note that the contributions created early in the pulse are being absorbed at the boundaries of the grid before the end of the pulse. Thus, the central part of the final momentum distribution in figure 2(a) is underestimated in this medium intensity case.

Before concluding, it is interesting to note and at present not understood that we observe contributions from the RESI process but none due to direct emission of the second electron upon rescattering in the first half of the pulse. The classical energy of the returning electron exceeds at least at $t = 2T$ the ionization limit, but there are no signatures of the creation of a correlated electron pair at this time instant at large center-of-mass momentum as in the later part of the pulse.

5. Conclusions

We have investigated how the concept of mapping ionization time to final momentum distribution can be extended from single ionization to time-resolved double ionization in strong fields. To this end, we have obtained the temporal evolution of the center-of-mass momentum from the numerical solutions of the TDSE of a fully correlated model atom. Simulations are performed in the medium and the high intensity regimes. Our results have shown that at high intensities the ionization dynamics is dominated by direct emission of the two electrons upon rescattering. Contributions from binary and recoil collision events are identified, the latter leading to unexpected large center-of-mass momenta of the two electrons. Both processes are also observed in the medium intensity regime, which are accompanied by contributions from the so-called RESI process. Deviations from the basic mapping principle as well as from the classical expectation of the correlated electron dynamics are discussed.

References

[1] Corkum P B and Krausz F 2007 *Nat. Phys.* **3** 381
[2] Goulielmakis E *et al* 2004 *Science* **305** 1267
[3] Itatani J, Levesque J, Zeidler D, Niikura H, Papin H, Kieffer J C, Corkum P B and Villeneuve D 2004 *Nature* **432** 867
[4] Agostini P and Di Mauro L F 2004 *Rep. Prog. Phys.* **67** 813
[5] Becker A, Dörner R and Moshammer R 2005 *J. Phys. B: At. Mol. Opt. Phys.* **38** S753
[6] Corkum P B 1993 *Phys. Rev. Lett.* **71** 1994
[7] Feuerstein B *et al* 2001 *Phys. Rev. Lett.* **87** 043003
[8] Becker A and Faisal F H M 2005 *J. Phys. B: At. Mol. Opt. Phys.* **38** R1
[9] Ruiz C, Plaja L, Roso L and Becker A 2006 *Phys. Rev. Lett.* **96** 053001

[10] Baier S, Ruiz C, Plaja L and Becker A 2006 *Phys. Rev.* A **74** 033405
[11] Weber Th *et al* 2000 *Phys. Rev. Lett.* **84** 443
[12] Moshammer R *et al* 2000 *Phys. Rev. Lett.* **84** 447
[13] Grobe R and Eberly J H 1992 *Phys. Rev. Lett.* **68** 2905
[14] Itatani J, Quere F, Yudin G L, Ivanov M Y, Krausz F and Corkum P B 2002 *Phys. Rev. Lett.* **88** 173903
[15] Mairesse Y and Quere F 2005 *Phys. Rev.* A **71** 0011401
[16] Staudte A *et al* 2007 *Phys. Rev. Lett.* at press
[17] Dörner R 2006 private communication